Structural Durability & Health Monitoring

Tech Science Press

https://doi.org/10.32604/sdhm.2026.077120

ARTICLE

Hybrid Effect of Steel Fiber and Rubber Powder on Freeze-Thaw Resistance and Pore Structure of Concrete

Wenwen Hu[1], Xinzhan Li[2], Tao Luo[2,*] and Li Li[2]

[1]Shaanxi Key Laboratory of Safety and Durability of Concrete Structures, Xijing University, Xi'an, China
[2]College of Water Resources and Architectural Engineering, Northwest A&F University, Yangling, China

*Corresponding Author: Tao Luo. Email: luotao19870426@126.com

Received: 02 December 2025; Accepted: 28 January 2026; Published: 18 May 2026

ABSTRACT: This study experimentally investigates the Hybrid Effect of Steel Fiber (SF) and Recycled Rubber Powder (RRP) on Freeze-Thaw (F-T) Resistance and Pore Structure of Concrete. With respect to the mechanical properties of Steel Reinforced Concrete (SRC) before and after F-T cycles, the mixture incorporating 1.5% SF and 10% RRP achieves the optimal performance, exhibiting a distinct positive hybrid effect with the γ of the tensile-to-compressive strength ratio of 1.427. The synergistic interaction between SF and RRP preserves the compressive strength and significantly enhances the tensile performance of SRC. Meanwhile, it alleviates the degradation of mechanical properties to a certain extent during 100–200 F-T cycles, enabling effective control over the mass loss and elastic modulus loss of SRC. Results from pore structure analysis reveal that SF and RRP exhibit a distinct negative hybrid effect on the porosity of SRC—a phenomenon that indicates the filling effect of RRP contributes to enhanced compactness of the concrete matrix.

KEYWORDS: Hybrid effect; steel fiber; recycled rubber powder; freeze–thaw cycles; mechanical properties; porosity

1 Introduction

In recent years, the development of sustainable construction materials has become a global research focus. Among various environmental challenges, the disposal of waste tires has emerged as a pressing issue worldwide [1–3]. It is estimated that over 4 billion end-of-life tires are currently stockpiled in landfills and storage facilities globally, with approximately 1.5 billion additional tires generated each year [4]. Incorporating waste tire rubber into concrete as a partial replacement for conventional raw materials not only addresses disposal concerns but also reduces the consumption of natural aggregates, thereby promoting sustainable development. Although the inclusion of RRP tends to reduce the compressive strength, flexural strength, and elastic modulus of concrete [5], it has been shown to improve several durability-related properties, such as impact resistance [6,7], abrasion resistance [8], and F-T resistance [9]. These enhancements highlight the need for further research into the characteristics and optimization of rubberized concrete for effective utilization of global solid waste resources [10].

In cold regions, concrete hydraulic structures are exposed to frequent F-T cycles due to low average annual temperatures and alternating wet–dry conditions. The increasing frequency of extreme low-temperature events and cold spells worldwide has further intensified this form of deterioration [11]. F-T cycling is one of the primary environmental factors leading to the degradation of concrete durability. During F-T cycles, water trapped in the internal pores of concrete undergoes repeated phase transitions: when the temperature drops below freezing, water expands to form ice crystals, generating substantial internal

tensile stress that exceeds the tensile strength of the concrete matrix, thereby initiating microcracks [12]. As the cycles proceed, these microcracks propagate and interconnect, further deteriorating the interfacial transition zone (ITZ) between aggregates and the cement matrix—an area inherently porous and weak [13]. The continuous deterioration of the ITZ weakens the bond between components, resulting in a significant decline in compressive strength, tensile performance, and elastic modulus of concrete over time. Previous studies have reported that RRP can improve the F–T resistance of concrete to a certain extent [14,15]. When incorporated at appropriate sizes and dosages, rubber particles improve the frost resistance, cracking resistance, and abrasion resistance of concrete [9]. In fact, rubberized concrete with optimized particle characteristics has been shown to exhibit F–T performance comparable to that of air-entrained concrete [16]. However, due to their high elasticity and chemical inertness, rubber particles do not participate in cement hydration and may create weak interfacial zones where microcracks initiate and propagate, which adversely affects the mechanical properties of concrete [7,15].

F-T damage in concrete primarily results from the accumulation of microcrack growth during cyclic freezing and thawing. In addition to improving internal pore structure, the inclusion of fibers has been widely adopted as an effective method to enhance the durability of concrete under F–T conditions [17–20]. SF is widely recognized for its crack-bridging effect, which can inhibit the initiation and propagation of microcracks in concrete, thereby improving toughness and tensile strength [21]. RRP, derived from waste tires, possesses excellent elastic properties that enable it to buffer internal stress induced by ice expansion during F-T cycles, reducing matrix damage [22]. However, the micro-scale synergistic mechanism between SF and RRP in improving concrete's F-T resistance is not yet fully understood. Existing studies have primarily focused on macro-mechanical performance, with limited insights into how RRP affects the interfacial bonding strength between SF and the matrix, and how SF compensates for the potential modulus reduction caused by RRP addition. For the micro-scale synergistic mechanism, we added specific elaboration: RRP, with its elastic properties, can buffer the internal stress caused by freeze-thaw cycles, reduce the damage to the matrix around SF, and thus improve the interfacial bonding strength between SF and concrete; meanwhile, SF can exert a bridging effect to inhibit the expansion of microcracks generated by RRP's low modulus, forming a complementary synergistic effect. This study aims to fill this research gap by systematically investigating the hybrid effect of SF and RRP on F-T resistance and pore structure of concrete, with a focus on clarifying the underlying micro-scale synergistic mechanism.

Beyond the advantages of enhanced mechanical properties and freeze resistance, the cost of the materials above warrants consideration. While SF-reinforced cementitious materials demonstrate superior mechanical performance, their relatively high cost limits applicability in conventional construction scenarios. In contrast, RRP functions as an efficient filling material; partial incorporation of RRP not only contributes to improving the comprehensive performance of SF-reinforced concrete but also reduces the required SF dosage, thereby naturally achieving a more favorable cost-performance ratio. Meanwhile, despite the relatively mature body of research on the single incorporation of SF or RRP, the synergistic mechanism underlying the hybrid use of these two materials—specifically its influence on concrete's mechanical properties and F-T resistance—requires further clarification. Furthermore, investigating the hybrid effect between SF and RRP holds significant implications for facilitating diversified material utilization and advancing waste recycling practices, aligning with the broader goals of sustainable construction.

Therefore, this study adopted a comprehensive modification strategy for concrete, integrating two F-T resistance enhancement methods: fine aggregate replacement with RRP and SF content adjustment. Experimental tests were conducted to evaluate key performance metrics of the modified concrete, including mass loss, elastic modulus, and mechanical properties (compressive strength, flexural strength, and splitting tensile strength), both prior to and following F-T cycling. Ultimately, the study discusses and establishes

the influence of the synergistic effect between SF and RRP on the mechanical properties and F-T resistance of concrete.

2 Experimental Procedures

2.1 Materials

In this study, P.O. 42.5 ordinary Portland cement with a specific surface area of 345 cm^2/g was used. The compressive and flexural strengths were 30.7 and 5.8 MPa at 3 days, and 50.9 and 8.6 MPa at 28 days, respectively. River sand with a fineness modulus of 2.89 and crushed gravel with a continuous grading of 5–20 mm were used as fine and coarse aggregates. The sand had a silt content of 1.65% and an apparent density of 2703 kg/m^3. Coarse aggregates were composed of 5–10 mm and 10–20 mm gravel mixed in a 4:6 ratio, with an apparent density of 2732 kg/m^3.

RRP, produced by shredding waste tires, was used to replace fine aggregates. The rubber had a particle size of 60 mesh (<250 μm), an apparent density of 750 kg/m^3 moisture content of (≤12.0%), and a 30-min closed filtration loss (≤40.0 mL). Copper-coated straight SF without hooked ends was used as reinforcement. The physical properties of the SF are presented in Table 1. Previous studies have shown that fiber incorporation can effectively mitigate F–T damage and enhance the performance of rubberized concrete [17,23]. Fig. 1 shows the morphology of the RRP and SF.

Table 1: Properties of steel fibers.

Steel Fiber	Length (mm)	Diameter (mm)	Tensile Strength (MPa)	Density (g/cm^3)
Copper-coated, straight	13 ± 2	0.22	3000	7.85

(a) (b)

Figure 1: Morphology of materials: (**a**) Steel fibers; (**b**) Recycled rubber powder.

2.2 Mix Proportions and Specimen Preparation

Concrete mix designs were based on the Chinese codes *JGJ 55-2011* (Specifications for Mix Proportion Design of Ordinary Concrete) and *GB 50119-2013* (Technical Code for Application of Concrete Admixtures). Considering that RRP does not contribute to hydration, volumetric replacement was used to maintain the overall cement paste ratio. Drawing upon recent studies [14] and considering engineering practice adaptability, the final research scope comprises 0%–2.0% steel fibers and 0%–15% recycled rubber powder. This facilitates comparative analysis with existing findings and has been validated as feasible through

preliminary experiments. To align with application scenarios and more clearly demonstrate the synergistic modification effects of SF and RRP, C50 concrete has been selected as the benchmark formulation.

RRP was used to replace 0%, 5%, 10%, and 15% of the fine aggregates by volume. On this basis, SF was added at 0%, 0.5%, 1.0%, 1.5%, and 2.0% by volume. Mix proportions are provided in Table 2. (In this study, when the proportion of steel fibers and recycled rubber powder in the mix design was relatively high, workability decreased. Therefore, the dosage of water-reducing agent was moderately increased to ensure workability met the requirements for moulding specimens.) The notation SnRmC refers to a concrete mix with *n*% SF and *m*% RRP (e.g., S0.5R5C represents 0.5% SF and 5% RRP).

Table 2: Concrete mix proportions.

Test Part Number	Water (kg/m^3)	Cement (kg/m^3)	Sand (kg/m^3)	Stone (kg/m^3)	Water Reducer (kg/m^3)	Gas-Inducing Agents (kg/m^3)	RRP (kg/m^3)	SF (kg/m^3)
S0R0C	136.8	340.8	461	1076	0.51	0.20	0	0
S0.5R0C	136.8	340.8	461	1076	0.51	0.20	0	39.25
S1.0R0C	136.8	340.8	461	1076	0.51	0.20	0	78.5
S1.5R0C	136.8	340.8	461	1076	0.51	0.20	0	117.75
S2.0R0C	136.8	340.8	461	1076	0.51	0.20	0	157
S0R5C	136.8	340.8	438	1076	0.51	0.20	11.50	0
S0.5R5C	136.8	340.8	438	1076	0.51	0.20	11.50	39.25
S1.0R5C	136.8	340.8	438	1076	0.51	0.20	11.50	78.5
S1.5R5C	136.8	340.8	438	1076	0.51	0.20	11.50	117.75
S2.0R5C	136.8	340.8	438	1076	0.51	0.20	11.50	157
S0R10C	136.8	340.8	415	1076	0.51	0.20	23.01	0
S0.5R10C	136.8	340.8	415	1076	0.51	0.20	23.01	39.25
S1.0R10C	136.8	340.8	415	1076	0.51	0.20	23.01	78.5
S1.5R10C	136.8	340.8	415	1076	0.51	0.20	23.01	117.75
S2.0R10C	136.8	340.8	415	1076	0.51	0.20	23.01	157
S0R15C	136.8	340.8	392	1076	0.51	0.20	34.51	0
S0.5R15C	136.8	340.8	392	1076	0.51	0.20	34.51	39.25
S1.0R15C	136.8	340.8	392	1076	0.51	0.20	34.51	78.5
S1.5R15C	136.8	340.8	392	1076	0.51	0.20	34.51	117.75
S2.0R15C	136.8	340.8	392	1076	0.51	0.20	34.51	157

After casting, the specimens were covered with plastic sheets and cured at 20 ± 5°C for 24 h. Then, they were transferred to a standard curing room at 20 ± 2°C and relative humidity ≥95% for 24 days. To ensure full water saturation before F-T testing, specimens were soaked in tap water for an additional 4 days.

Specimens for compressive and splitting tensile strength tests were prepared in 100 mm × 100 mm × 100 mm cubes, and those for flexural tests were 100 mm × 100 mm × 400 mm prisms.

2.3 Rapid F-T Test

F-T cycling was performed according to *GB/T 50081-2016* (Standard for Mechanical Properties of Ordinary Concrete), *CECS 13:2009* (Standard Test Method for Fiber-Reinforced Concrete), and *GB/T 50082-2009* (Standard Test Method for Long-Term and Durability Properties of Ordinary Concrete).

The freezing and thawing durations were set to 1.0–2.5 h and 1.0–2.0 h, respectively. The minimum and maximum temperatures during the cycles were −16.0°C and 3.0°C. The heating phase exceeded one-quarter of the total F–T cycle duration. Freezing stage (from 3.0°C to −16.0°C): the corresponding temperature change rate is 10°C/h; Heating stage (from −16.0°C to 3.0°C): the temperature change range is also 19.0°C, and the corresponding temperature change rate is 14°C/h. A TD-R28 rapid F-T testing machine (produced by Tianjin Gangyuan Testing Instruments Co., Ltd.) was used.

2.4 Testing Methods

Mechanical tests were conducted using an MTS Exceed E63 universal testing machine (2000 kN capacity, precision class 0.5), manufactured by MTS Industrial Systems Co., Ltd. The relative errors in force and displacement measurements were within ±0.5%. The stress rate range was 1–30 MPa/s, and the strain rate range was 0.00025–0.025/s.

2.4.1 Compressive Strength Test

Cubic specimens (100 mm × 100 mm × 100 mm) were tested after 0, 50, 100, 150, and 200 F–T cycles. A load-controlled mode was adopted, with a loading rate of 0.6 MPa/s.

2.4.2 Splitting Tensile Strength Test

Splitting tensile tests were conducted on the same size cubic specimens (100 mm × 100 mm × 100 mm) after the same F–T cycles, using a loading rate of 0.06 MPa/s.

2.4.3 CT Scanning and Pore Structure Analysis

To investigate the influence of rubber content and SF dosage on F-T resistance, selected concrete specimens with varying rubber replacement levels and fiber contents were scanned using a CT system at different F–T cycle stages. The CT scan employed a pixel resolution (PixelDis) of 0.139 mm and a voxel resolution (VoxelDis) of 0.102713 mm; Three parallel specimens were prepared for each mix design (150 mm × 150 mm × 150 mm cubic specimens subjected to freeze-thaw cycles). The analysis volume was set to 1200 × 1200 × 1200 voxels (corresponding to approximately 123.26 mm × 123.26 mm × 123.26 mm), with a subregion size of 1024 × 1024 pixels. Image processing steps in Avizo software: First, median filtering (3 × 3 neighbourhood, consistent with parameter RectR = 3) and outlier pixel removal (StdVar = 3.0) were performed for noise reduction. Subsequently, segmentation was conducted using a dual-threshold method (matrix threshold: 120–255, pore threshold: 0–50) for segmentation, combined with manual correction to eliminate artefacts; finally, the visualisation module extracts three-dimensional pore parameters (porosity, equivalent diameter, connectivity) to analyse porosity evolution.

2.5 Evaluation of the Influence of Hybrid Effect on F-T Performance

To better quantify the impact of the hybrid effect of SF and RRP with different dosages on the F-T resistance of SRC, this study introduces the enhancement factor and hybrid effect factor for further analysis, based on the research findings of Banthia and Li [24,25].

Herein, β is defined as the enhancement coefficient, and γ as the hybrid effect factor, with their calculation formulas given in Eqs. (1) and (2):

$$\beta = \frac{S}{S_m} \tag{1}$$

where: S = F-T resistance index of concrete enhanced by SF and RRP; S_m = F-T resistance index of plain concrete without SF and RRP. S is a single metric representing the evaluation indicator for changes in properties, such as mass loss, elastic modulus, and mechanical performance, after freeze-thaw cycles, as they vary with the dosage of SF or RRP. When calculating for a specific formulation, only the performance characteristics of that formulation and its control group are considered. The control group must be selected such that either SF or RRP is the sole variable, thereby isolating the individual reinforcing effect of each material.

$$\gamma_{A-B} = \frac{\beta_{A-B}}{\beta_A \cdot \beta_B} \tag{2}$$

where: γ_{A-B} = hybrid enhancement coefficient of concrete with both SF and RRP; β_A = enhancement factor when only SF is incorporated; β_B = enhancement factor when only RRP is incorporated.

A value of $\gamma > 1$ indicates a positive hybrid effect, while $\gamma < 1$ indicates a negative hybrid effect. The hybrid effect factor can reflect the influence of the hybrid effect of SF and RRP (with different dosages) on the F-T resistance of SRC. A larger hybrid effect factor implies a more significant improvement in the F-T resistance of SRC (incorporating both fibers and RRP) compared to concrete with only SF or only RRP.

3 Results

3.1 Mass Loss and Relative Dynamic Modulus of Elasticity

The variations of mass loss ratio (*Wn*) and relative dynamic modulus of elasticity (*Pn*) with increasing F–T cycles for the concrete specimens are presented in Fig. 2. For all specimen groups, both mass loss and *Pn* deterioration significantly increased as the number of F–T cycles rose. Based on these two indicators, the optimal dosage ranges for SF and RRP were determined to be approximately 1.5% and 10% by volume, respectively.

(1) The incorporation of RRP effectively mitigated mass loss, *Wn*, and *Pn*. When the RRP content exceeded 5%, the mass loss after 200 cycles approached the limiting value of 5.0%. Specifically, for the control group without SF (S0RmC), the mass loss and RDME stabilized at approximately 4% and 94% after 200 F–T cycles. Compared with the reference mix with 0% RRP, the mixes with 5%, 10%, and 15% RRP replacement exhibited reductions in mass loss of approximately 12.5%, 51.8%, and 65.6%, respectively, and *Pn* improvements of about 10.1%, 17.9%, and 20.8%, respectively. This improvement is attributed to the similarity in particle size between fine aggregates and the RRP, which acts similarly to air-entraining agents in enhancing the F–T resistance of concrete [26], and the hydrophobic effect of rubber, which can reduce the water absorption capacity of the concrete matrix, decrease the content of free water inside the specimen, and further inhibit ice formation and volume expansion during freeze-thaw cycles.

When SF was incorporated, the addition of RRP further enhanced the F-T resistance. Compared to the corresponding mixes without RRP (SnR0C), the mixes with 5%, 10%, and 15% rubber powder (SnR5C, SnR10C, SnR15C) exhibited decreases in mass loss of 1%–2% and increases in RDME of approximately 8%–10%. Moreover, as the RRP content increased, the differences in *Wn* and *Pn* among mixes with varying SF contents gradually diminished, with the smallest differences observed at 10% RRP replacement.

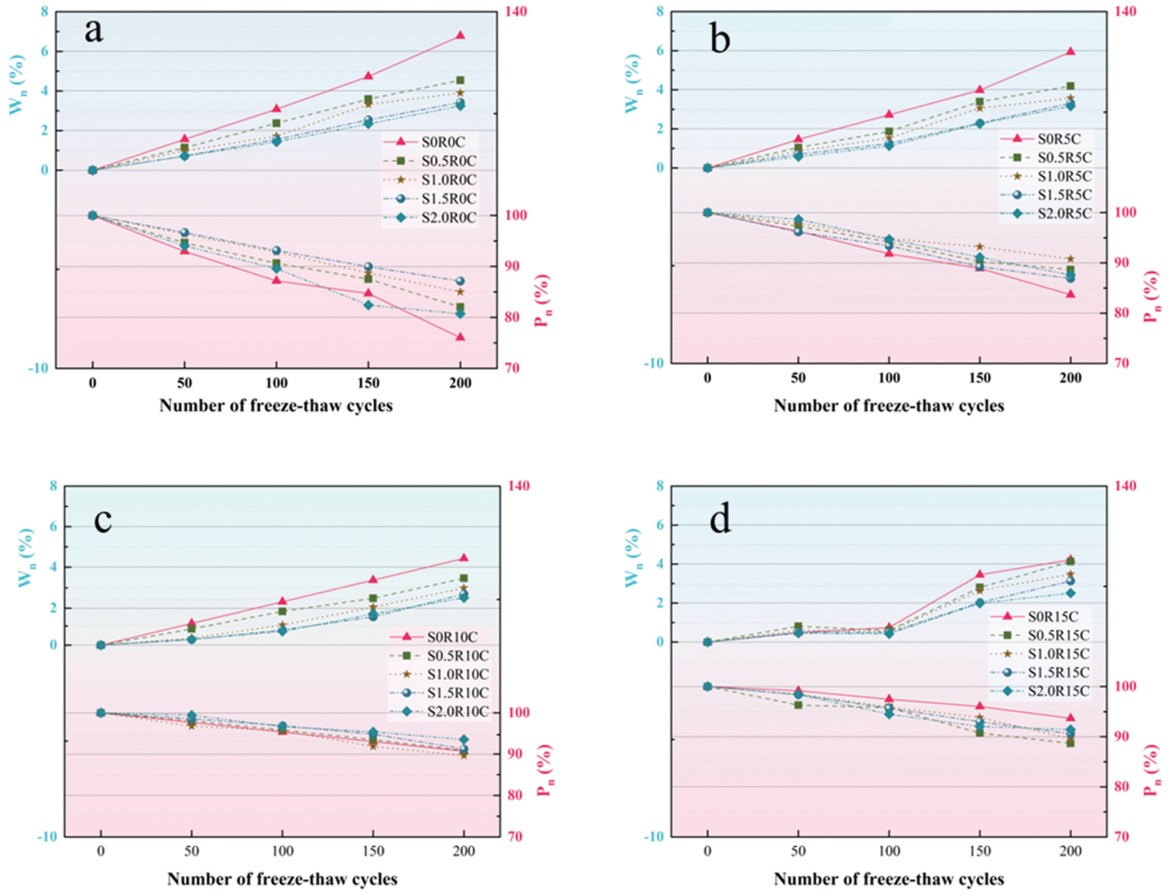

Figure 2: Evolution of mass loss and relative dynamic modulus of elasticity with increasing F-T cycles for: (**a**) SnR0C; (**b**) SnR5C; (**c**) SnR10C; (**d**) SnR15C.

The fine particle size of RRP effectively fills internal pore defects, enhancing specimen density. Additionally, RRP particles are non-absorbent and hinder water ingress into smaller pores, reducing the overall water absorption rate of the specimens. The introduction of numerous micro-closed air bubbles further impedes free water penetration by surface tension effects, thereby collectively improving F-T durability.

(2) SF addition also retarded the degradation of *Wn* and *Pn*, although its effect diminished with increasing RRP powder content. Within the SnR0C group, SF dosages of 0.5%, 1.0%, 1.5%, and 2.0% reduced mass loss by 33.04%, 63.44%, 86.15%, and 103.22%, and increased *Pn* by 7.93%, 10.96%, 13.08%, and 5.38%, respectively, compared to the control without fiber (S0). This indicates that SF effectively bridge and transfer stresses, suppressing the formation and propagation of large cracks induced by F-T cycles. Notably, under varying RRP contents, SF dosages of 1.5% and 2.0% consistently yielded similar and optimal F-T resistance. This suggests that the optimal fiber content for minimizing *Wn* and maximizing *Pn* lies within this range. However, considering economic viability, an SF dosage of 1.5% is deemed the optimal proportion.

3.2 Compressive Strength

All specimens exhibited reductions in compressive strength with increasing F–T cycles. Furthermore, compressive strength decreased with higher RRP replacement, despite significant improvements in F-T durability. The addition of SF partially compensated for the strength loss and enhanced F-T performance. Considering workability, compressive strength, and F-T resistance, the optimal dosages were approximately 1.5% SF and 15% RRP.

3.2.1 Effect of SF

For each RRP replacement level, compressive strength before and after F–T followed the order: S0RmC < S0.5RmC < S1.0RmC < S2.0RmC < S1.5RmC. From a steel fiber dosage perspective, 1.5% fiber yielded the highest strength. Higher dosages (>1.5%) led to fiber agglomeration during mixing, resulting in poor workability. Therefore, 1.5% fiber was optimal.

Fig. 3a shows the compressive strength evolution of SnR0C specimens: before F–T, mixes with 0.5%, 1.0%, 1.5%, and 2.0% fiber increased strength by 5.8%, 20.7%, 26.15%, and 23.8% compared to S0R0C. After 200 cycles, strength reductions were 54.7%, 27.5%, 18.1%, 14.1%, and 14.0%, respectively. Similar trends were observed for SnR5C (Fig. 3b), SnR10C (Fig. 3c), and SnR15C (Fig. 3d), with increasing SF content improving strength retention after F-T. Overall, the addition of SF constrained crack propagation and enhanced compressive strength, with an optimum dosage around 1.5%. During the mixing process of concrete with SF content exceeding 1.5%, obvious fiber agglomeration—SFs tended to clump together rather than disperse uniformly in the matrix, forming local fiber clusters. Strength decreased due to fiber agglomeration increasing internal porosity and weak fiber–matrix interfaces caused by elastic modulus mismatch.

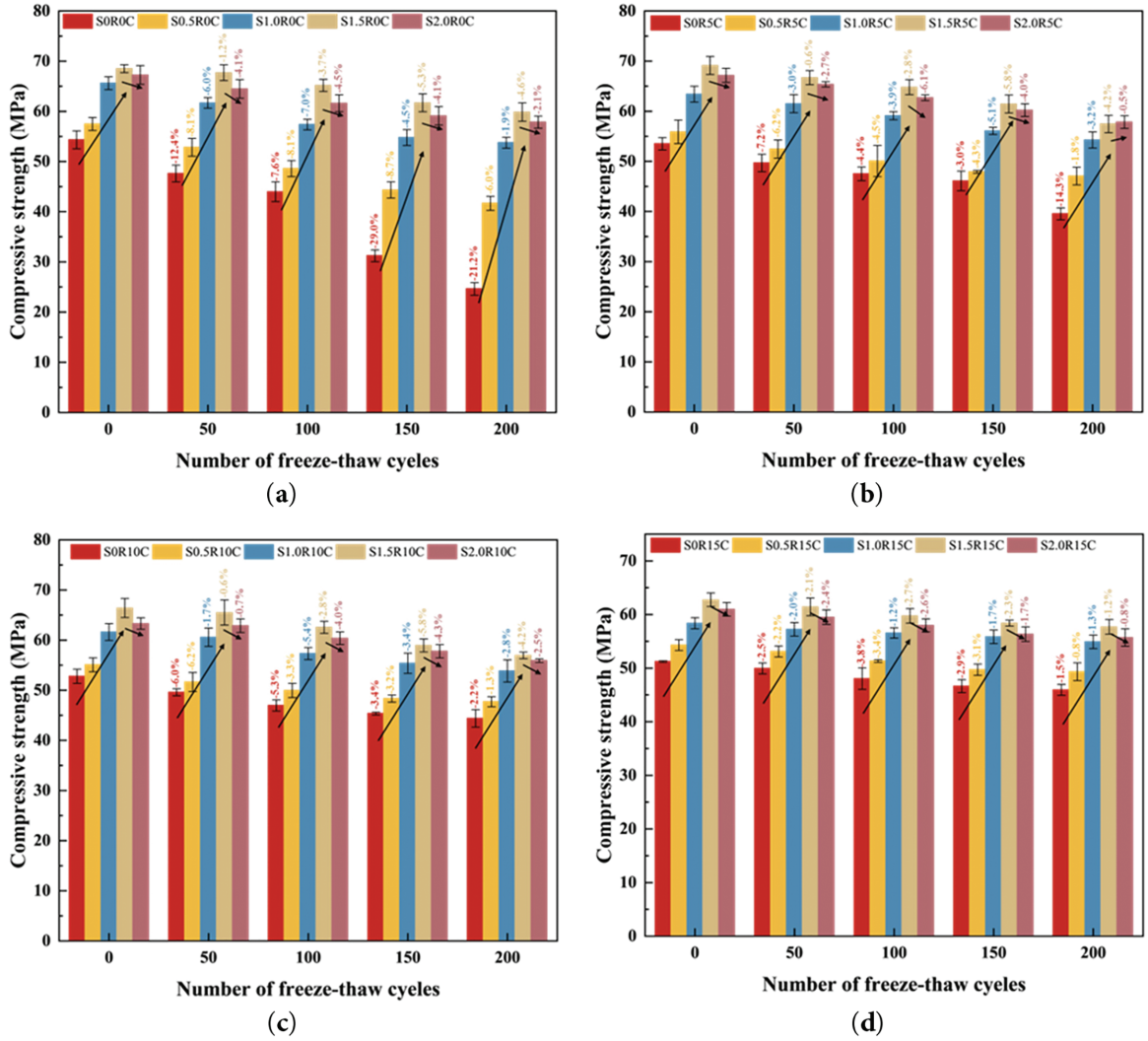

Figure 3: Evolution of compressive strength with increasing F-T cycles for: (**a**) SnR0C; (**b**) SnR5C; (**c**) SnR10C; (**d**) SnR15C. (Numbers indicate percentage strength reduction every 50 cycles relative to the previous measurement).

3.2.2 Effect of RRP

Before F–T, compressive strength of S0R5C, S0R10C, and S0R15C decreased by approximately 1.5%, 2.8%, and 5.7% compared to S0R0C, respectively. After 200 cycles, strength reductions were 54.7%, 26.2%, 15.9%, and 10.3%, respectively. Similar strength degradation patterns were observed for other fiber content groups. The strength decrease is attributed to RRP's hydrophobic nature and poor bonding with cement paste, resulting in weak interfaces prone to microcracking under compressive load. Notably, after 50 F–T cycles, specimens with RRP powder maintained strengths above 50 MPa, outperforming the control mix without RRP. From 50 to 150 cycles, the control group showed marked strength deterioration (up to 29%), while RRP-containing mixes exhibited mitigated degradation. This demonstrates that recycled RRP powder significantly alleviates F-T damage on compressive strength, with higher RRP content further reducing strength loss.

The improved F-T resistance is explained by RRP powder's smaller particle size filling pores that aggregates cannot fill, increasing specimen density and reducing internal defects. This limits water ingress during F-T cycles, preventing damage from free water expansion.

3.3 Splitting Tensile Failure Patterns

This section analyzes the failure patterns of concrete specimens from the S0RmC group after 0, 100, and 200 F-T cycles, and compares them with specimens from the SnR10C group after 200 cycles. The results demonstrate that RRP significantly enhances the frost resistance of concrete, while the addition of SF effectively restrains crack propagation during failure.

At peak splitting tensile load, the S0R0C specimens exhibited abrupt failure accompanied by a loud cracking sound, indicating brittle behavior (Fig. 4). When the RRP content was low (≤5%), the failure patterns were similar to those of plain concrete. As the RRP content increased (≥10%), the cracking sound during failure was noticeably reduced, with the sound diminishing further with higher RRP contents. Moreover, the specimens did not fracture into separate pieces. At a 10% RRP content, multiple fine cracks appeared upon failure, with significantly reduced width in the primary crack.

After 100 F-T cycles, the failure mode remained predominantly brittle. Specimens failed suddenly at peak load, splitting into two parts along a single straight-through crack. However, at higher RRP contents (≥10%), despite a rapid reduction in load-bearing capacity at peak load, the specimens remained intact, and multiple secondary cracks developed around the main crack. Unlike the uncycled specimens, the main cracks tended to curve, suggesting a transition toward ductile failure. As F-T cycles increased, visible surface damage became more prominent. After 200 cycles, conventional concrete specimens exhibited surface aggregate exposure and spalling. In contrast, specimens with 10% RRP replacement showed more extensive cracking and signs of ductile failure. At 15% RRP content, the overall integrity after splitting was significantly improved, with finer cracks distributed across the specimen surface.

With increasing SF content, the loud cracking sound during failure disappeared, replaced by faint fracture noises. Cracks transitioned from a single dominant fracture to multiple thin, tortuous ones. At peak load, the specimens did not lose load-bearing capacity instantly but displayed clear ductile failure behavior. As the differences in crack morphology among the four RRP content groups were relatively minor, only the failure patterns of SnR10C specimens are presented here. The bridging effect of SF preserved the integrity of the specimens post-failure, promoted the development of multiple microcracks, and redirected the crack paths. The cracks propagated from the center toward the edges, reflecting the surface-to-core damage progression induced by F-T cycling. At 0.5% to 1.0% SF content, some cracks penetrated the entire specimen; at 1.5%, no through-cracks were observed post-failure. However, at 2.0% SF content, excessive

dosage weakened the interfacial bond between fibers and matrix under F-Tconditions, causing microcracks to merge and extend rapidly during loading.

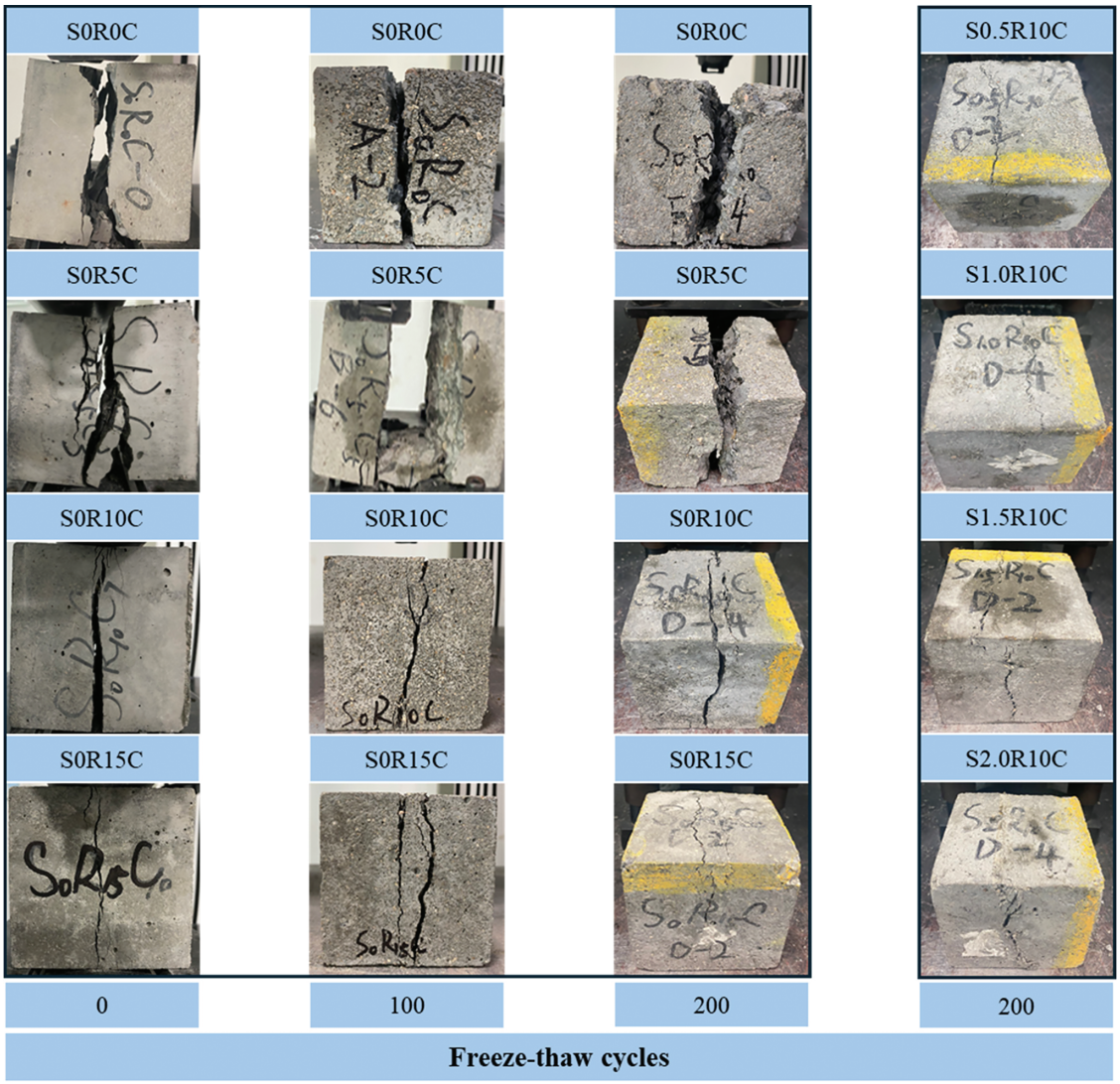

Figure 4: Comparison of splitting tensile failure modes of specimens subjected to different numbers of F-T cycles.

3.4 Splitting Tensile Strength

The splitting tensile strength of the specimens generally decreased with increasing F-T cycles. However, a slight increase in splitting tensile strength was observed with higher replacement rates of RRP, accompanied by a significant improvement in F-T resistance. The incorporation of SF further enhanced both the splitting tensile strength and F-T durability of the concrete matrix. Interestingly, a synergistic enhancement effect between SF and RRP on splitting tensile strength was observed in this study. The results after 200 F-T cycles indicate that the strength degradation was effectively mitigated. Considering workability, tensile strength, and F-T resistance in combination, the optimal contents of SF and RRP were determined to be 1.5% and 10%, respectively.

3.4.1 Effect of Steel Fibers

The splitting tensile strength of concrete specimens with varying RRP replacement ratios at different F-T stages is presented in Fig. 5. Within the SnR0C group, the addition of SF led to strength improvements of 24.94%, 28.62%, 50.41%, and 60.94% for fiber dosages of 0.5%, 1.0%, 1.5%, and 2.0%, respectively, compared to the plain S0R0C specimen before F-T cycling. After 200 F-T cycles, the corresponding strength reductions were 52.30%, 36.51%, 27.52%, 19.02%, and 21.60%, indicating that higher fiber content (≥1.5%) significantly enhanced tensile strength and mitigated F-T deterioration.

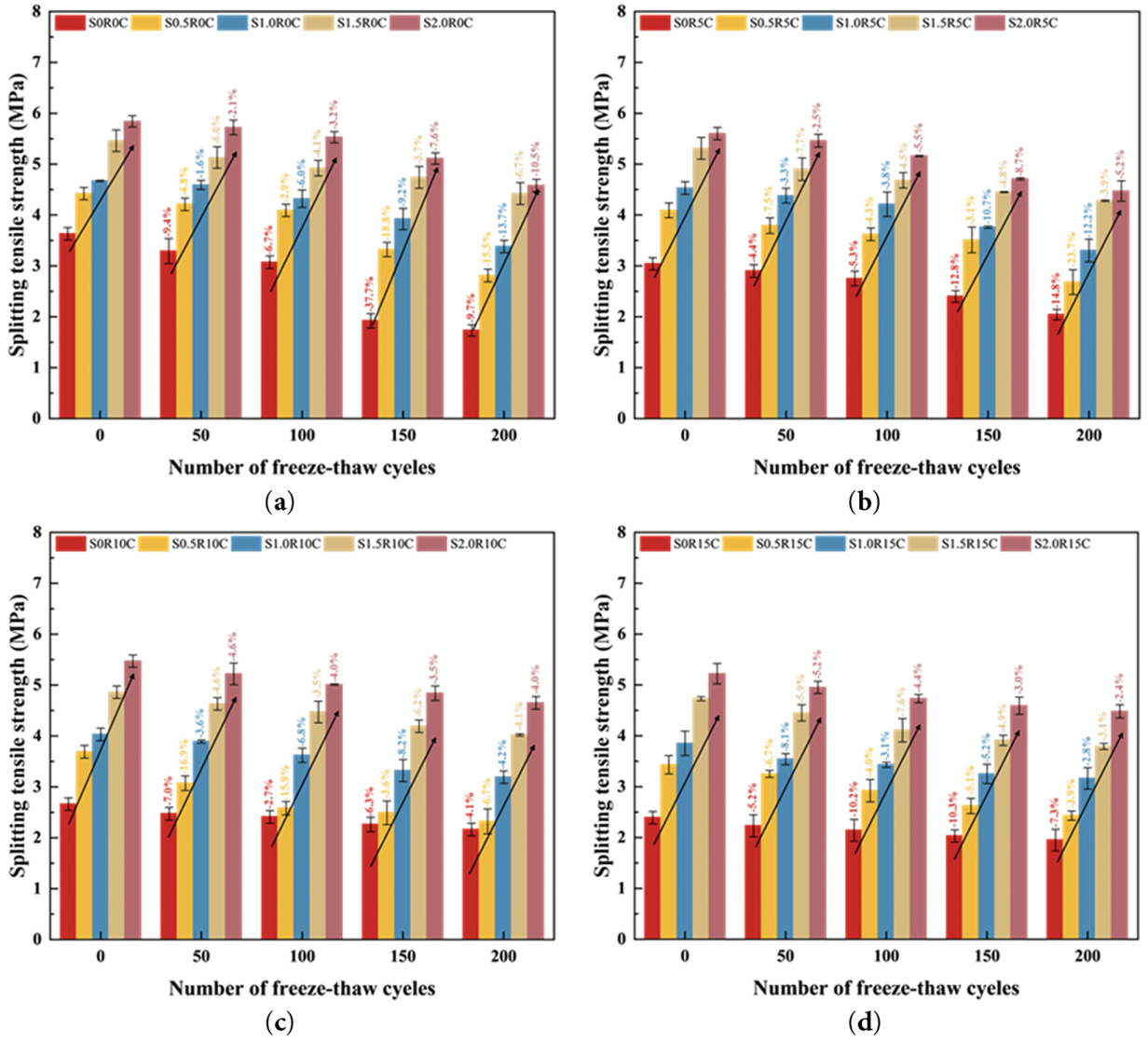

Figure 5: Evolution of splitting tensile strength measurements with increasing F-T cycle counts: (**a**) SnR0C; (**b**) SnR5C; (**c**) SnR10C; (**d**) SnR15C. (The numbers in the figure represent the decrease in splitting tensile strength of the test specimen relative to the previous measurement after every 50 F-T cycles).

At lower fiber contents (≤1.0%), the internal fiber network was insufficient to form an effective constraint system. As a result, when tensile stress was applied, the crack network tended to bypass the SF and propagate along weaker interfaces. Conversely, when the fiber dosage reached or exceeded 1.5%, a stable restraining

network formed within the concrete matrix, significantly improving the splitting tensile strength. Under axial loading, the initial failure occurred at the cement–aggregate interface. The presence of SF introduced tensile resistance at these interfaces, constraining crack development and limiting failure propagation.

A similar trend was observed in the SnR5C, SnR10C, and SnR15C groups. Prior to F-T cycling, the addition of SF enhanced tensile strength by approximately 34.83%–84.55%, 38.72%–105.63%, and 43.51%–118.41%, respectively. After 200 cycles, all fiber-reinforced specimens retained higher tensile strength than their fiber-free counterparts. For example, in the SnR15C group, strength reductions after 200 cycles were 18.59%, 29.13%, 17.90%, 19.96%, and 14.17% for SF contents of 0%, 0.5%, 1.0%, 1.5%, and 2.0%, respectively. Notably, while a 0.5% fiber content effectively improved tensile capacity prior to cycling, it was insufficient to inhibit Freeze-Thaw-induced matrix damage, leading to the most pronounced post-cycling strength loss—this trend was also evident in the other RRP groups.

The enhanced tensile strength in SRC can be attributed to the stress-bridging and crack-arresting effects of the SF. However, at low dosages, the fibers cannot effectively absorb the stress concentrations induced by F-T cycles, allowing cracks to rapidly propagate under tensile loads. Only with sufficient fiber content can the internal stress be redistributed effectively, thereby limiting crack growth and improving resistance to frost damage.

3.4.2 Effect of RRP

Throughout the F-T testing process, it was observed that when the RRP replacement ratio was relatively low (≤5%), the reduction in splitting tensile strength progressively increased with the number of cycles. However, at higher replacement levels (≥10%), the rate of strength loss diminished as the number of F-T cycles increased. The evolution of splitting tensile strength in the S0RmC group is shown in Fig. 5. Before F-T cycling, the tensile strengths of the S0R5C, S0R10C, and S0R15C specimens were reduced by 16.3%, 36.7%, and 34.1%, respectively, compared to plain concrete. After 200 F-T cycles, the strength reductions were 52.3%, 32.8%, 18.7%, and 18.6% for the S0R0C, S0R5C, S0R10C, and S0R15C groups, respectively.

The evolution of splitting tensile strength in the S0.5RmC, S1.0RmC, S1.5RmC, and S2.0RmC groups is also illustrated in Fig. 5. Before F-T exposure, compared to specimens without RRP (SnR0C), the addition of RRP led to reductions in splitting tensile strength ranging from 4% to 34%. As the SF content increased, this loss was mitigated. Specifically, in the 2.0% fiber group, the strength reduction due to RRP was limited to 4%–10.6%.

After 200 F-T cycles, the splitting tensile strength reductions in the S0.5RmC, S1.0RmC, S1.5RmC, and S2.0RmC groups were in the ranges of 36.5%–29.1%, 27.5%–17.9%, 20.0%–17.2%, and 21.6%–14.2%, respectively. In the S2.0RmC group, the strength ranking after cycling was S2.0R5C < S2.0R15C < S2.0R0C < S2.0R10C. The remaining groups exhibited similar trends to those observed in S0RmC.

These results indicate that moderate amounts of RRP can reduce the loss of splitting tensile strength caused by F-T damage. However, due to the hydrophobic nature of RRP and its weak bonding with the cement matrix, the effective load-bearing area is diminished. As a result, the overall strength of the concrete is slightly reduced. The inclusion of RRP particles increases the proportion of weak interfaces within the specimen, thus decreasing the effective stress-transfer area under tensile loading. Nevertheless, this trade-off is counterbalanced by the enhanced frost resistance provided by the RRP, especially when combined with SF.

3.5 Tensile-to-Compressive Strength Ratio

The tensile-to-compressive strength ratio of concrete, defined as the ratio of splitting tensile strength to compressive strength, serves as an indicator of structural safety and stability [27,28]. A higher ratio

implies better performance in terms of ductility and resistance to brittle failure, thereby reflecting enhanced material toughness.

As shown in Fig. 6, the incorporation of SF significantly increases the tensile-to-compressive strength ratio. The improvement is most pronounced when the fiber content is between 1.5% and 2.0%. For the reference group without SF, the ratio ranges from 0.04 to 0.07. When the SF content reaches 2.0%, the ratio increases to 0.096–0.108, representing an enhancement of 61%–145% compared to the control. When the fiber dosage is below 1.0%, the effect is marginal, indicating that a low SF content has limited influence on improving the tensile-to-compressive strength ratio of ultra-high-performance concrete. When the fiber content exceeds 1.0%, the improvement becomes more significant due to better fiber dispersion and stronger fiber–matrix bonding, which enhances the concrete's stability and resistance to brittle fracture.

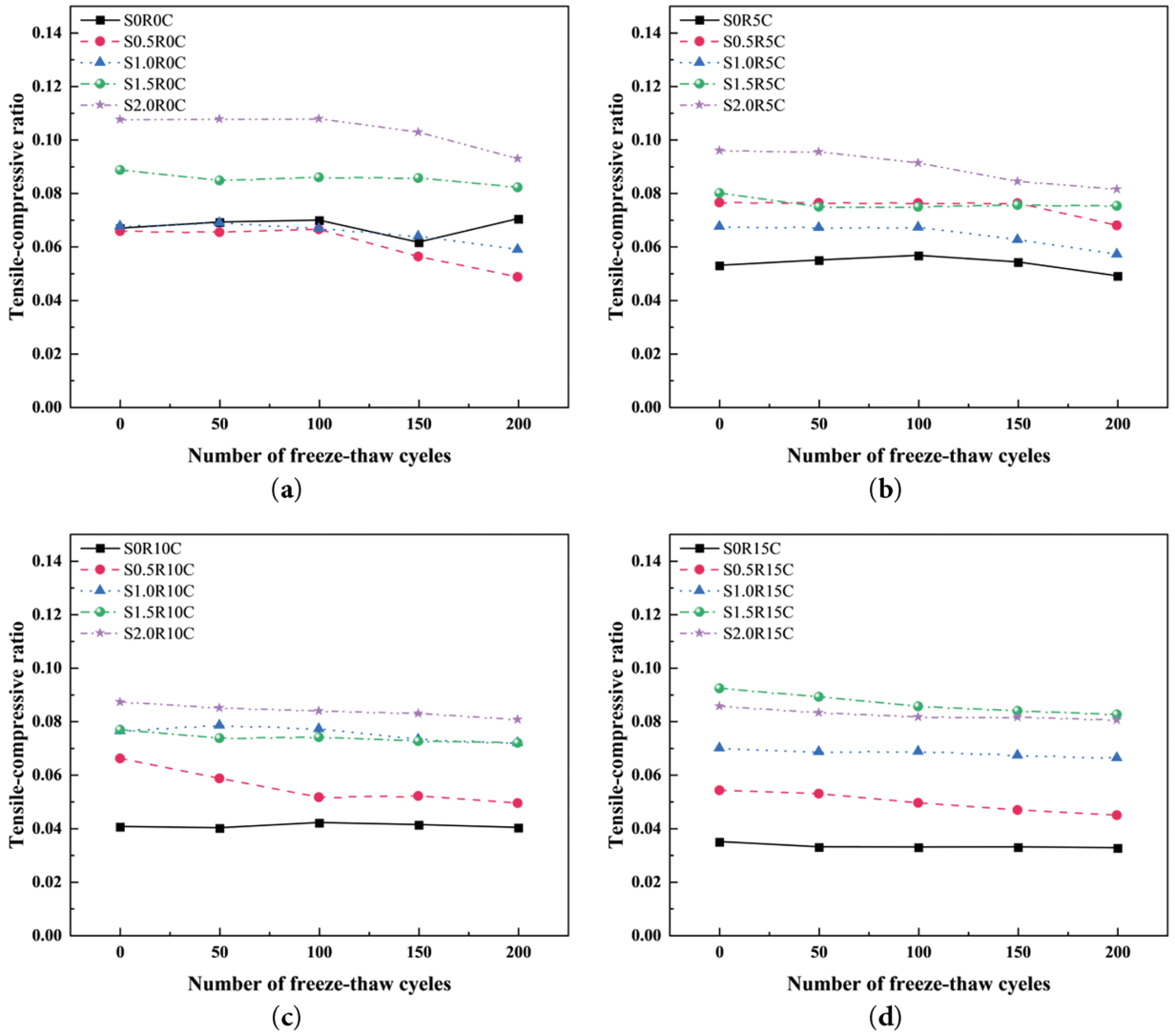

Figure 6: Evolution of splitting tensile strength measurements with increasing F-T cycles: (**a**) SnR0C; (**b**) SnR5C; (**c**) SnR10C; (**d**) SnR15C.

On the other hand, the inclusion of RRP tends to reduce the tensile-to-compressive strength ratio, as illustrated in Fig. 7. In plain concrete without SF, increasing the RRP content from 0% to 15% results

in a 48.8% reduction in the tensile-to-compressive ratio, indicating a significant deterioration in ductility. This trend persists across different SF dosages. However, the negative effect of RRP on the ratio is partially mitigated by increasing SF content. At 15% RRP replacement, the tensile-to-compressive ratio first increases and then decreases with increasing fiber content, showing variations of 17.7%, 3.5%, 4.2%, and –20.4% for SF contents of 0.5%, 1.0%, 1.5%, and 2.0%, respectively. These findings suggest that a SF dosage of 1.0%–1.5% is optimal for enhancing the tensile-to-compressive strength ratio, while excessive RRP content should be avoided to prevent brittle fracture.

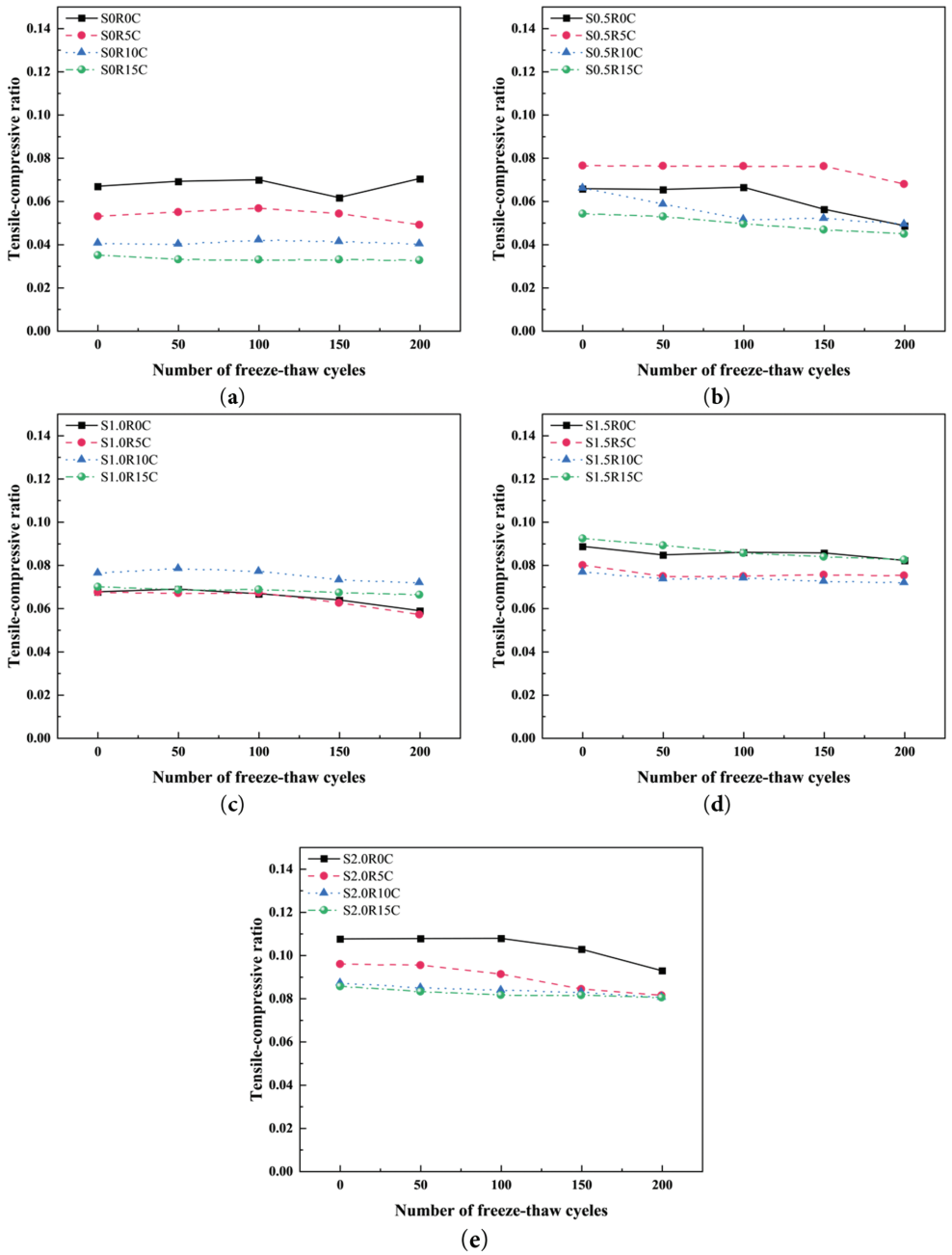

Figure 7: Evolution of tensile-compressive ratio measurements with increasing F-T cycle counts: (**a**) S0RmC; (**b**) S0.5RmC; (**c**) S1.0RmC; (**d**) S1.5RmC; (**e**) S2.0RmC.

3.6 Porosity

At a fixed RRP replacement level, the porosity of concrete increases with the SF content, particularly when the dosage exceeds 0.5%. Although the addition of SF raises the porosity, it also reduces the rate of porosity increase under F-T cycles, indicating that SF helps mitigate F-T damage to some extent.

CT scans (Fig. 8) reveal that the initial pore distribution was relatively dispersed, but F-T cycles expanded the internal pores, resulting in a high concentration of voids after 200 cycles. The evolution of porosity for different SF contents at each RRP dosage is shown in Fig. 9. For SnR0C specimens, Fig. 9a illustrates that before F-T cycling, adding 0.5% SF increases porosity by only 2.3% compared to plain concrete. However, porosity increases significantly with higher fiber contents: 30.3%, 105.6%, and 204.5% for fiber contents of 1.0%, 1.5%, and 2.0%, respectively. After 200 F-T cycles, porosity in specimens with 0%, 0.5%, 1.0%, 1.5%, and 2.0% SF content increased by 61.5%, 79.3%, 77.9%, 58.3%, and 42.3%, respectively.

Fig. 10 illustrates the evolution of porosity for varying RRP contents at a fixed SF dosage. In S0RmC specimens (Fig. 10a), RRP significantly optimized the pore volume. Before F-T cycles, specimens with 5%, 10%, and 15% RRP showed porosity reductions of 8.9%, 13.8%, and 16.9% compared to plain concrete. CT images confirm that RRP helps control pore size distribution, yielding more small pores and maintaining stable pore structures even after F-T exposure. RRP particles likely act as cushions, absorbing expansion-induced energy and preventing microcrack formation.

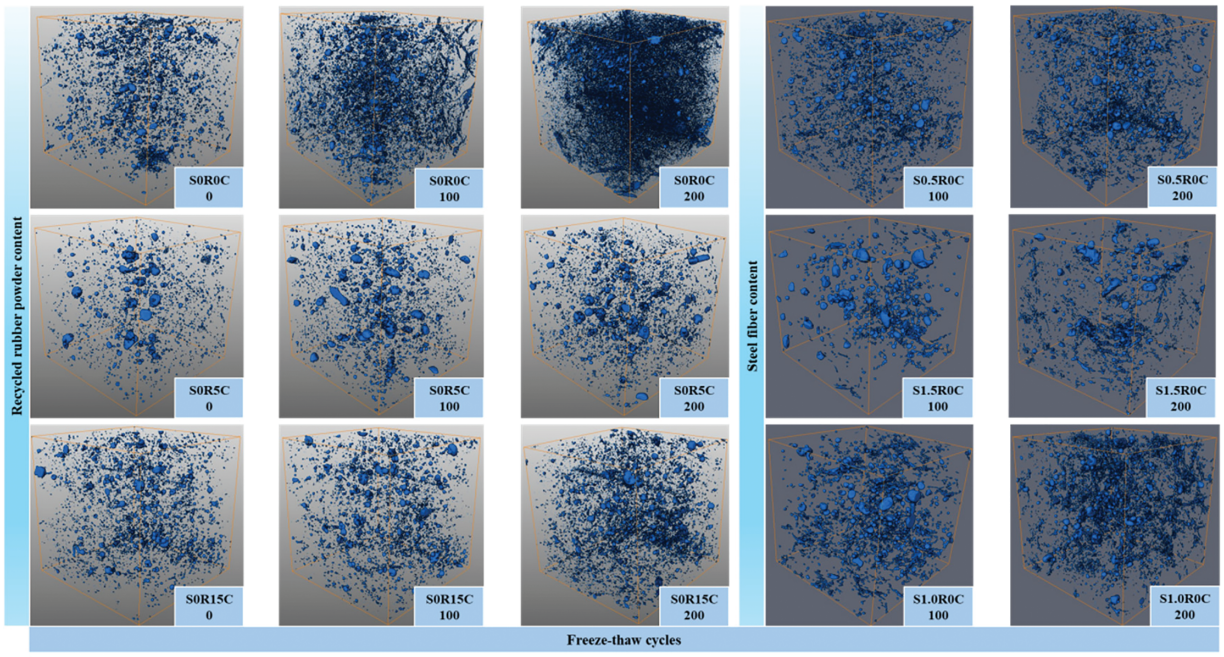

Figure 8: CT images of pore structure in selected concrete specimens.

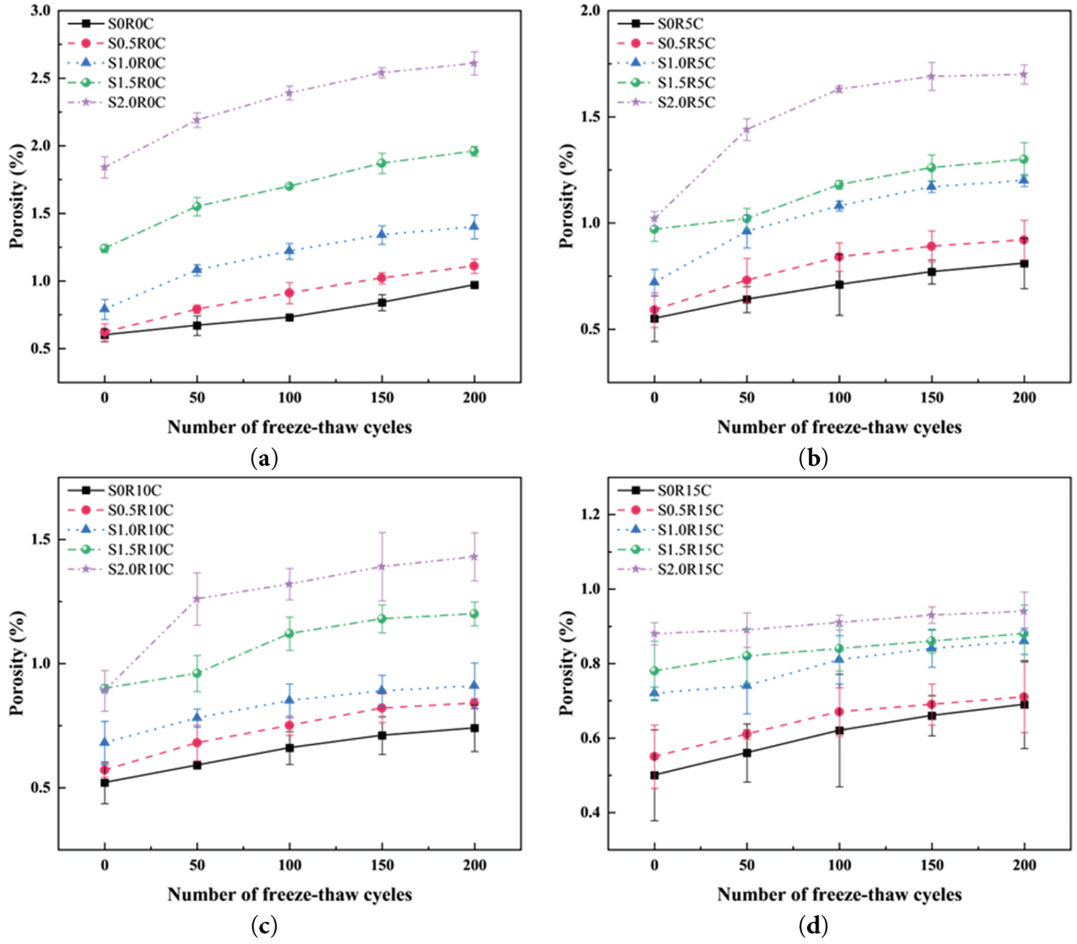

Figure 9: Porosity evolution under increasing F-T cycles: (**a**) SnR0C; (**b**) SnR5C; (**c**) SnR10C; (**d**) SnR15C.

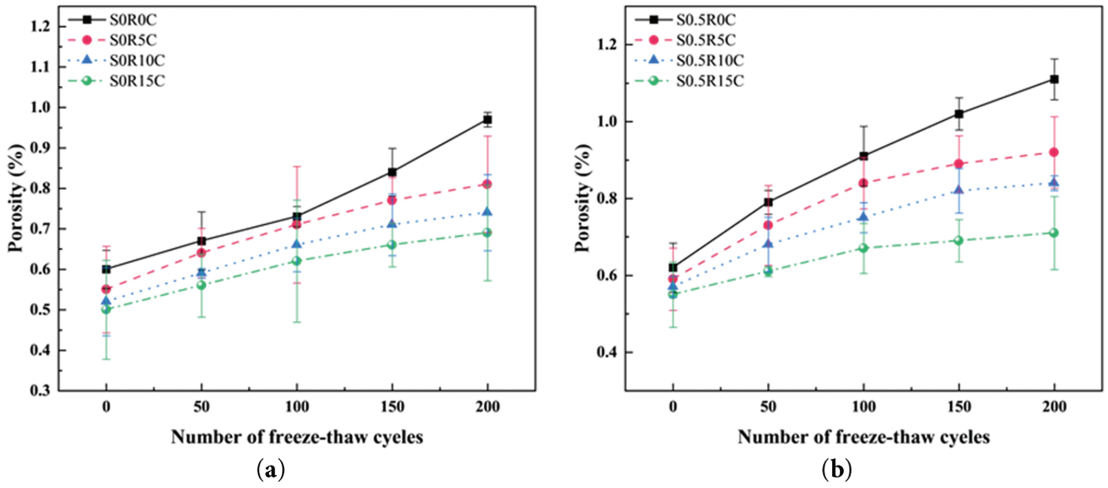

Figure 10: (Continued)

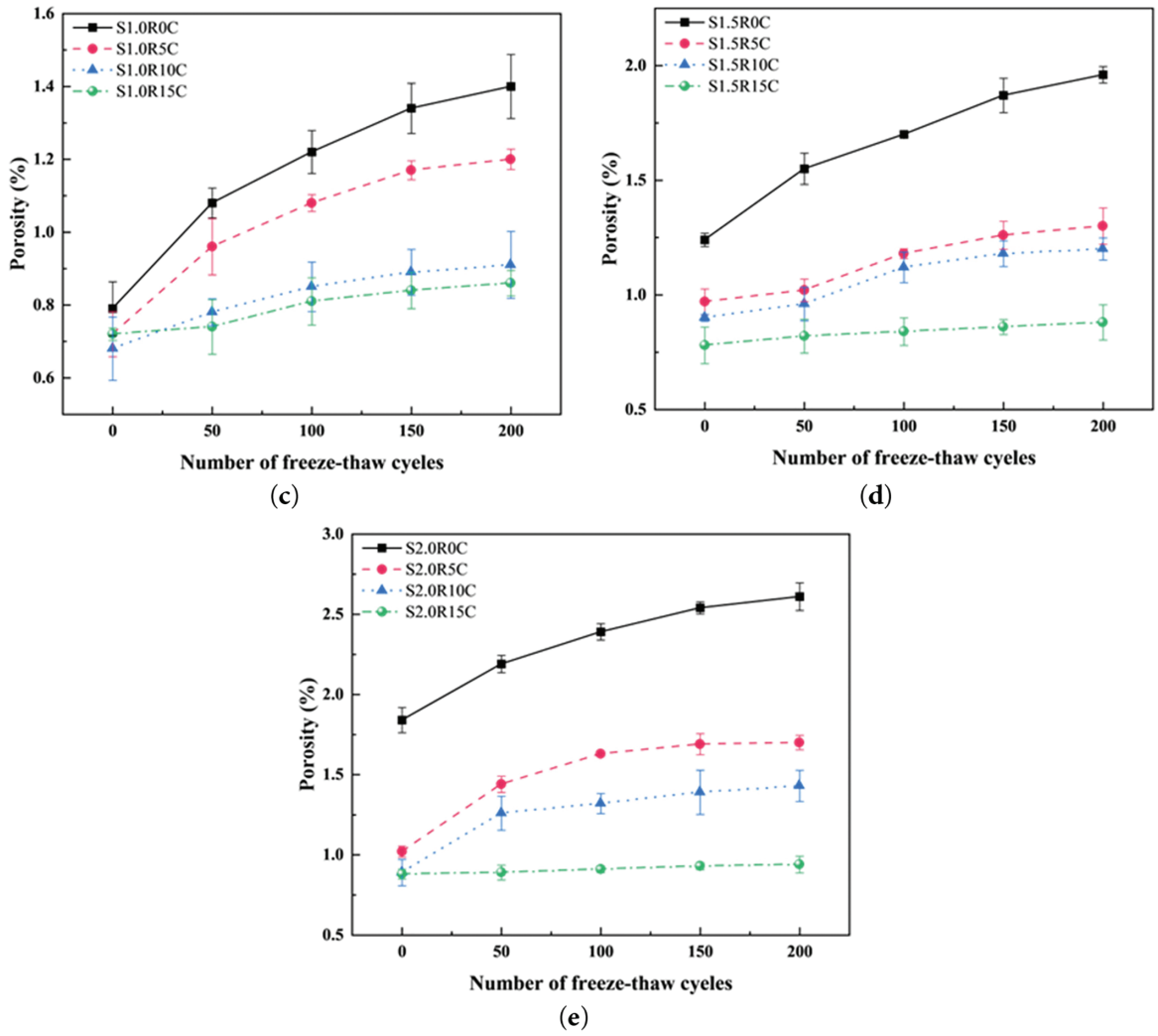

Figure 10: Porosity evolution under increasing F-T cycles at constant SF contents: (**a**) S0RmC; (**b**) S0.5RmC; (**c**) S1.0RmC; (**d**) S1.5RmC; (**e**) S2.0RmC.

For plain concrete, porosity increases sharply with more F-T cycles. With RRP, however, the rate of porosity increase slows, suggesting a stabilizing effect. RRP's smaller particle size allows it to fill internal voids more effectively, enhancing compaction and density. Moreover, the inclusion of RRP introduces stable closed microbubbles that help relieve internal pressure caused by water expansion, further improving F-T durability.

Despite the increase in porosity with SF addition, F-T resistance improved due to the bridging effect of fibers (Fig. 11), which helped resist internal stresses from pore water pressure, crystallization pressure, and frost suction pressure. The fibers also suppressed crack propagation, partially compensating for the porosity-related weaknesses.

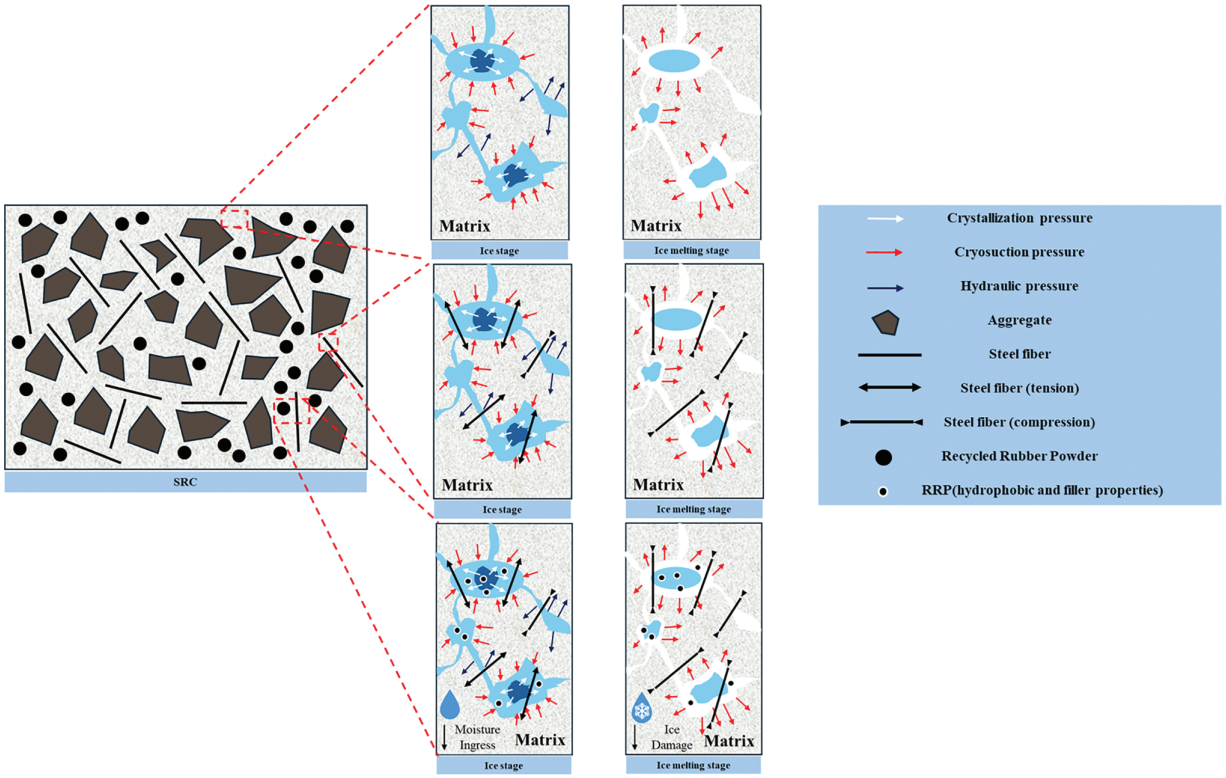

Figure 11: Schematic diagram of the synergistic crack-resistance mechanism between SF and RRP during F-T cycles.

3.7 Synergistic Effect of SF and RRP on Concrete Performance

3.7.1 Compressive Strength

As shown in Fig. 12a, without F-T cycles, the γ of compressive strength was greater than 1 (indicating a positive hybrid effect) only when the SF content was 1.5% or 2.0%, and the RRP content was 0%. This suggests that the hybrid effect of SF and RRP has a limited role in improving compressive strength. At low RRP contents, the γ of compressive strength for SRC exhibited an upward trend with increasing SF incorporation. This is mainly attributed to the fact that the addition of SF increases the energy dissipation of concrete under compressive failure. When the SF content was fixed, the overall γ of compressive strength decreased with the increase in RRP content, which may be attributed to excessively weak interface zones between RRP and concrete, resulting in a negative hybrid effect. When RRP and SF were used simultaneously, the compressive strength decreased more significantly, and the negative hybrid impact between the two became more prominent. This is due to three factors: the deteriorated workability of concrete, the substantial increase in weak interface zones within the concrete, and the limited contribution of RRP to improving the compressive strength of concrete. However, when the SF content was 1.5%, the γ of compressive strength reached its maximum value of 1.019, while the γ loss value was also the largest. This indicates that even with a relatively high SF content, the combination of fibers and RRP still further reduces the compressive strength of SRC. In contrast, when the SF content was 2.0%, SF could restrict concrete cracking through the fiber-matrix bonding effect, thereby preventing significant losses in concrete compressive strength.

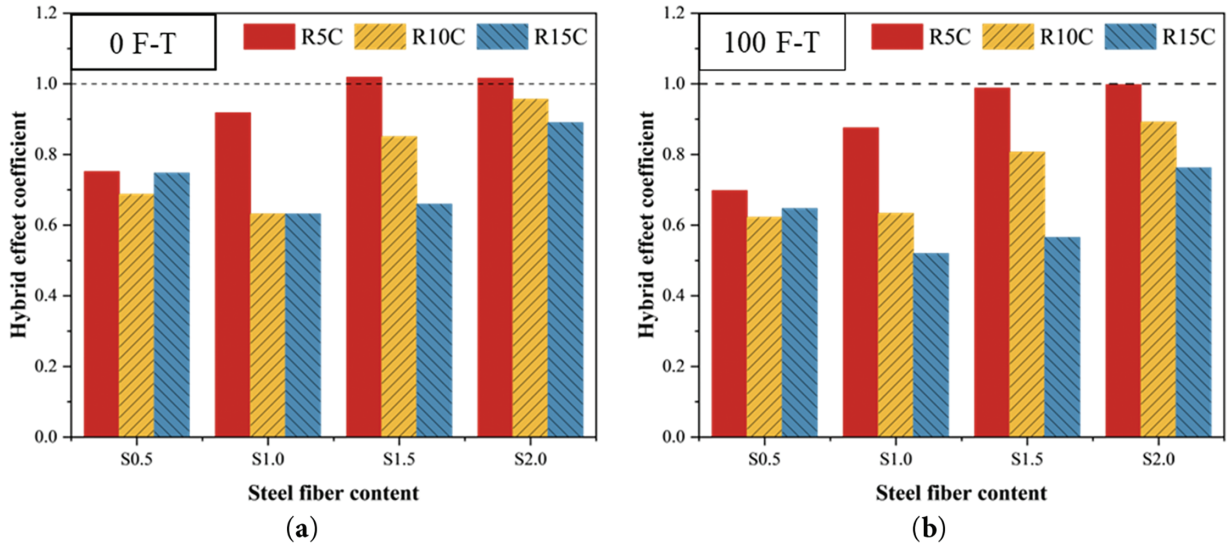

Figure 12: Relationship between the hybrid effect coefficient (γ) of compressive strength and steel fiber (SF) content: (**a**) 0 F-T; (**b**) 100 F-T.

As shown in Fig. 12b, after 100 F-T cycles, the γ for compressive strength exhibited a slight decrease compared to that before F-T cycling, with all groups showing $\gamma < 1$. At low RRP contents, the γ value displayed a positive correlation with the increasing SF content; however, when the SF content exceeded 1.0%, the improvement effect became limited. This indicates that a high SF content not only significantly enhances the compressive performance of concrete before F-T cycling but also maintains a certain degree of enhancement in compressive performance after F-T cycling. At high RRP contents, the variation trend of γ was similar to that before F-T cycling: an increase in SF content could significantly inhibit the negative hybrid effect of RRP. This is attributed to the fiber bridging effect, which restricts the development of cracks in concrete during F-T cycles. Nevertheless, an increase in RRP content reduced the hybrid effect of SF and RRP, failing to achieve a comprehensive improvement in the compressive performance of concrete. Through the analysis of the hybrid impact of SF and RRP on compressive strength, it is concluded that a low RRP content combined with a relatively high SF content can comprehensively enhance the compressive strength of SRC. The optimal contents are determined as 1.5%–2.0% for SF and 5% for RRP, respectively.

3.7.2 Splitting Tensile Strength

As shown in Fig. 13a, without F-T cycling, the γ of splitting tensile strength for SRC was greater than 1, indicating a positive hybrid effect. This phenomenon is mainly attributed to two factors: first, the continuous incorporation of SF endows concrete with a certain tensile strength through the fiber bridging effect; second, the small particle size of RRP enables it to effectively fill some internal voids in the concrete paste, improve the interfacial behavior of the matrix, and thus enhance the tensile strength. When the SF content was fixed, the γ value increased significantly with the increase in RRP content. This may be due to the gradual filling of pores introduced by SF, which makes the concrete matrix tend to be denser—a conclusion that the earlier discussion on porosity can support. When the RRP content was fixed, the γ value also increased with the increase in SF content; however, when the RRP content was 5%, the enhancement effect was limited due to the insufficient pore-filling capacity of RRP at this dosage. When RRP and SF were used simultaneously, the positive hybrid effect between the two became more prominent. Specifically, when the SF content was 2.0%, the γ of splitting tensile strength reached the maximum value of 1.358. This indicates that under the

condition of relatively high SF content, the combination of fibers and RRP further improves the splitting tensile strength of SRC. The underlying mechanism lies in the fact that, at a relatively high RRP content, RRP enhances the compactness of the concrete matrix by filling voids, which in turn improves the bonding performance between SF and the matrix, ultimately ensuring the overall enhancement of the concrete's splitting tensile strength.

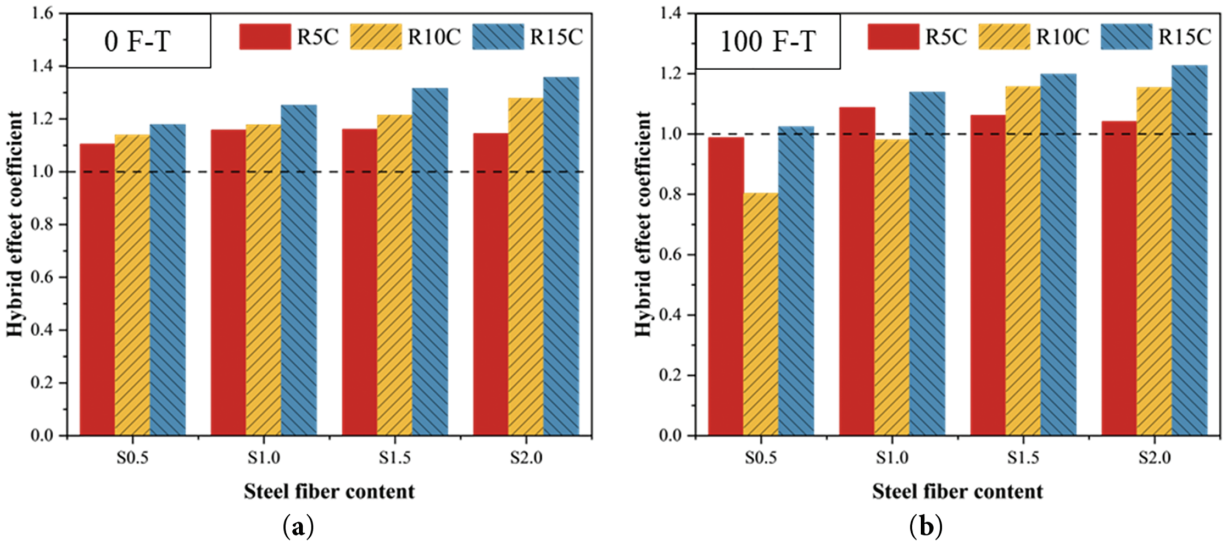

Figure 13: Relationship between the hybrid effect coefficient (γ) of splitting tensile strength and steel fiber (SF) content: (**a**) 0 F-T; (**b**) 100 F-T.

However, after 100 F-T cycles, the γ of splitting tensile strength decreased significantly compared to that before F-T cycling, and some test groups even showed γ < 1, as presented in Fig. 13b. At high RRP contents, the γ value exhibited a positive correlation with the increasing SF content. This indicates that despite the F-T exposure, the combination of high RRP content and SF can still exert a synergistic effect to enhance the splitting tensile performance of concrete. Meanwhile, at high RRP contents, the variation trend of γ was consistent with that observed before F-T cycling: an increase in SF content could notably promote the hybrid effect of RRP. This is attributed to the fiber bridging effect, which effectively inhibits the initiation and propagation of cracks in concrete during F-T cycles. Through the analysis of the hybrid impact of SF and RRP on the splitting tensile strength of SRC, it is concluded that a low SF content combined with a relatively high RRP content can comprehensively enhance the splitting tensile strength of SRC. The optimal dosages are determined to be 1.5%–2.0% for SF and 10%–15% for RRP, respectively.

3.7.3 Tensile-to-Compressive Strength Ratio

As shown in Fig. 14a, the γ of the tensile-to-compressive strength ratio induced by SF and RRP were all greater than 1, indicating a positive hybrid effect. This implies that the combination of SF and RRP can significantly improve the toughness of SRC, with a more notable enhancement compared to the single incorporation of either material. The primary mechanism behind this phenomenon is that the addition of RRP enables SRC to form a relatively denser structure between SF and the surrounding matrix during tensile failure, thereby significantly improving its tensile performance. In contrast, RRP has a limited effect on enhancing compressive performance. This difference in the influence of RRP on tensile and compressive properties directly contributes to the increase in the tensile-to-compressive strength ratio. When the SF content was fixed, the γ of the tensile-to-compressive strength ratio increased with the increase in RRP

content. Specifically, when the SF content was 1.5%, the γ of the tensile-to-compressive strength ratio reached its maximum value of 1.995. This is likely because, in SRC with a relatively high SF content, the RRP fills most of the interface zones between SF and the matrix, effectively restricting the initiation and propagation of cracks and thus exhibiting an excellent hybrid synergy. However, the combination of 2.0% SF content and RRP failed to achieve an effective hybrid effect. This may be attributed to the fact that an excessively high SF content compensates for the loss of compressive strength (caused by RRP), while the improvement in splitting tensile strength (driven by the SF-RRP synergy) is relatively limited, resulting in a reduced enhancement of the tensile-to-compressive strength ratio compared to the 1.5% SF group.

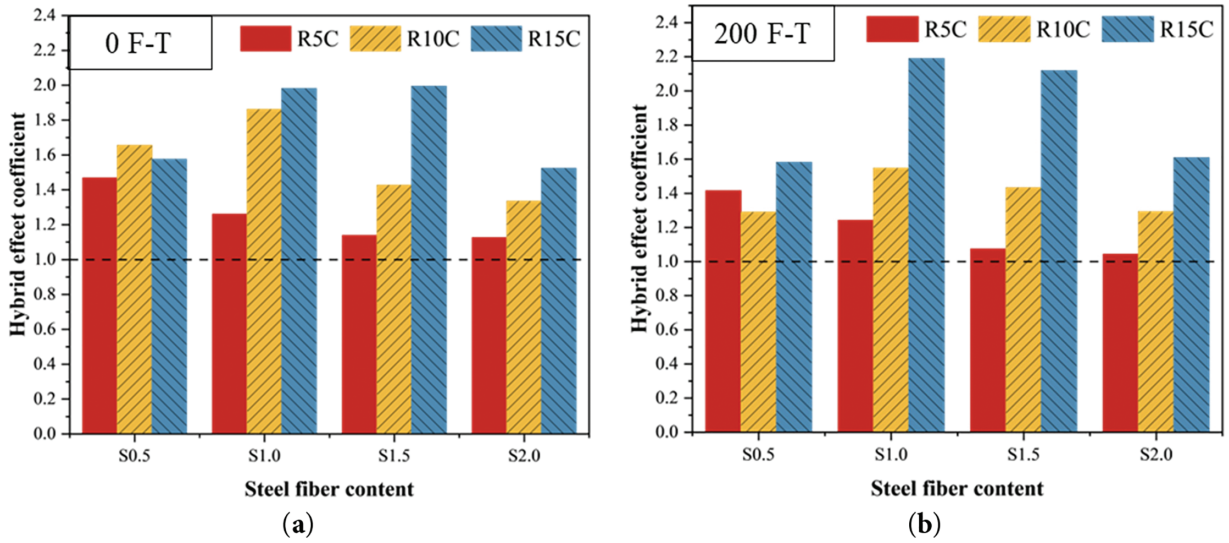

Figure 14: Relationship between the hybrid effect coefficient (γ) of the tensile-to-compressive strength ratio and steel fiber (SF) content: (**a**) 0 F-T; (**b**) 200 F-T.

After 100 F-T cycles, the γ of the tensile-to-compressive strength ratio remained greater than 1 for all groups, with no significant decrease compared to the pre-F-T state, as presented in Fig. 14b. At low RRP contents, the γ value exhibited a decreasing trend with increasing SF content. When the RRP content exceeded 5.0%, the hybrid effect first increased and then decreased as the SF content increased. This phenomenon indicates that at low RRP contents, the concrete matrix undergoes more severe damage after F-T cycling; in contrast, at high RRP contents, the variation trend of γ was consistent with that observed before F-T cycling. This is attributed to the filling property of high RRP content, which can effectively inhibit the initiation and propagation of cracks in concrete during F-T cycles. Through the analysis of the hybrid effect of SF and RRP on the tensile-to-compressive strength ratio of SRC, it is concluded that a reasonable combination of SF and RRP can comprehensively enhance the tensile-to-compressive strength ratio of SRC. The optimal dosages are determined to be 1.0%–1.5% for SF and 10%–15% for RRP, respectively.

3.7.4 Porosity

As shown in Fig. 15, without F-T cycling, the γ of porosity was greater than 1 (indicating a positive hybrid effect) only when the SF content was 1.5% or 2.0%. With the continuous incorporation of SF, the γ of porosity for SRC showed a significant upward trend—particularly at high SF contents, where the increase in γ was remarkably prominent. This phenomenon is primarily attributed to the fact that the incorporation of SF tends to introduce additional pores into the concrete during the mixing process. However, as the RRP content in SRC increases, RRP can effectively fill the pores within the concrete; this filling effect becomes

more pronounced, especially at high SF contents (where SF generates more pores). When the SF content was 1.5%, the γ of porosity reached its maximum value of 1.28. Meanwhile, within the same SF content group, the magnitude of γ loss also increased most significantly with the rise in RRP content. This indicates that under the condition of relatively high SF content, the synergistic effect between SF and RRP can effectively reduce the porosity of concrete and ensure the compactness of the matrix. Nevertheless, when the SF content reached 2.0%, the pore-filling effect of RRP was weakened—possibly due to the excessive number of pores introduced by the ultra-high SF content, which exceeded the filling capacity of RRP.

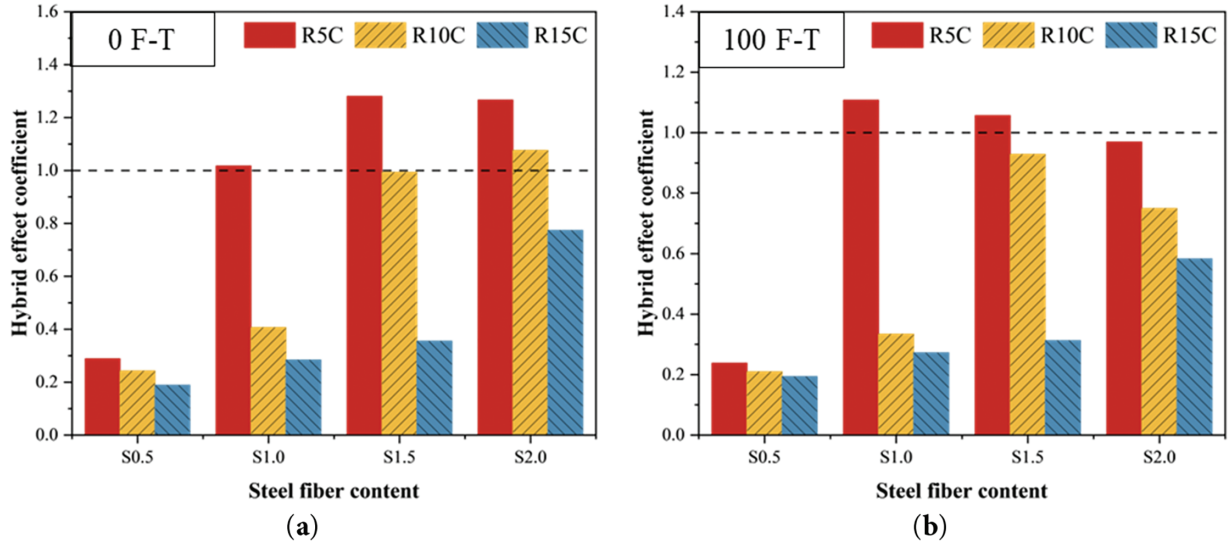

Figure 15: Relationship between the hybrid effect coefficient (γ) of porosity and steel fiber (SF) content: (**a**) 0 F-T; (**b**) 100 F-T.

After 100 F-T cycles, the γ of porosity exhibited a notable change compared to that before F-T cycling. Specifically, at low RRP contents, the γ value first increased and then decreased with the increasing SF content. This observation indicates that although the incorporation of SF significantly enhances the mechanical properties of concrete during F-T cycling, the damage to the pore structure of concrete (i.e., increased porosity) becomes relatively more pronounced after F-T cycling. In contrast, RRP can inhibit the generation of such additional pores. At high RRP contents, the variation trend of γ was consistent with that observed before F-T cycling. This is attributed to the filling effect of RRP, which renders the concrete matrix relatively dense and thereby suppresses the development of pores in concrete during F-T cycles. Through the analysis of the hybrid effect of SF and RRP on the porosity of SRC, it is concluded that a reasonable combination of SF and RRP can effectively reduce the porosity of SRC and further enhance its resistance to F-T-induced pore damage. The optimal dosages are determined to be 1.5% for SF and 15% for RRP, respectively.

3.8 Life-Cycle Assessment Considering Freeze–Thaw Damage

A service-oriented LCA was performed to evaluate S1.5R10C under F–T exposure. Material-stage accounting yields an embodied cost of 333.32 RMB/m^3 and embodied carbon of 297.37 kg CO_2-eq/m^3 for the reference S0R0C, and 1100.08 RMB/m^3 and 533.79 kg CO_2-eq/m^3 for S1.5R10C. Experimental results show S1.5R10C retains >70% of mechanical properties after 200 F–T cycles; accordingly, a conservative service-life extension factor of 2.0 is adopted for S1.5R10C (i.e., equivalent required volume = 0.50 m^3 to deliver the same long-term function). Under this durability adjustment, the life-cycle (equivalent) impacts become

550.04 RMB/m^3 and 266.89 kg CO_2-eq/m^3 for S1.5R10C, vs. 333.32 RMB/m^3 and 297.37 kg CO_2-eq/m^3 for the reference. Thus, although life-cycle cost increases by ~65.0%, embodied carbon decreases by ~10.2%. These results indicate that durability gains from the SF–RRP synergy can offset upfront embodied emissions, yielding net life-cycle carbon benefits despite higher initial material cost. Sensitivity to the assumed service-life factor is noted; full LCCA, including maintenance and user costs, will further strengthen the case for the hybrid system in severe F–T environments.

4 Discussion

This study confirms that the combined incorporation of SF and RRP produces a synergistic improvement in the F-T durability of C50 concrete by integrating microstructural optimisation with macroscopic crack control. The optimal dosage of 1.5% SF and 10% RRP achieves a balanced enhancement of durability-related properties, reflecting the complementary roles of the two modifiers. The optimal mix ratio (1.5% SF + 10% RRP) is suitable for load-bearing structures in severe cold regions, such as water conservancy and road projects, which are susceptible to freeze-thaw damage. RRP contributes primarily through capillary pore refinement and hydrophobic effects, reducing porosity by 22.5% and effectively limiting moisture ingress and ice-induced damage, as evidenced by mass loss below 3% after 200 freeze–thaw cycles. The stiffness reduction associated with rubber inclusion is offset by SF, which bridges microcracks and enhances post-cracking toughness, enabling elastic modulus retention exceeding 75%. The observed decline in compressive strength at higher fiber contents further confirms the existence of a critical fiber dosage threshold in composite systems. From a damage evolution perspective, RRP predominantly mitigates early-stage deterioration related to moisture transport, whereas SF restrains late-stage stiffness degradation driven by crack accumulation. Their coupled action establishes a coherent synergistic pathway linking pore-scale regulation and crack-bridging reinforcement to improved freeze–thaw resistance. Despite the lack of explicit characterisation of rubber surface properties and fiber dispersion, the results clarify the intrinsic mechanism governing the durability enhancement. Overall, this work refines the mechanistic understanding of SF–RRP composite modification and provides a rational basis for designing freeze–thaw-resistant concrete incorporating recycled rubber.

5 Conclusions

This study systematically investigated the hybrid effect of SF and RRP on the F-T damage characteristics and mechanical properties of concrete after F-T cycles. The main conclusions are as follows:

(1) RRP can significantly improve the F-T resistance of concrete and effectively alleviate the deterioration of concrete's mechanical properties (compressive strength and splitting tensile strength) caused by F-T cycles. However, it should be noted that the incorporation of RRP results in an approximate 5%–10% strength loss of concrete before F-T cycles, reflecting a trade-off effect between the F-T resistance and the initial strength of concrete.

(2) With the increase in SF content, the compressive strength of concrete shows a variation law of "first increasing and then decreasing". After 200 F-T cycles, the S1.5R15C specimen (incorporating 1.5% SF and 15% RRP) exhibits the optimal compressive strength, reaching 57.7 MPa. SF inhibits the propagation of macro-cracks through the fiber bridging effect and induces the generation of dispersed micro-cracks inside concrete to dissipate energy. Specifically, when the SF content is 1.5%, the concrete can retain more than 70% of its initial mechanical properties after 200 F-T cycles, demonstrating excellent F-T stability.

(3) The synergistic effect of SF and RRP enables a significant enhancement in both the mechanical properties and F-T resistance of concrete. This hybrid effect not only ensures a lower mass loss rate and elastic modulus loss rate under the same number of F-T cycles but also exerts a remarkably positive impact on improving the splitting tensile strength and tensile-to-compressive strength ratio of the material. Notably,

compared with the sole incorporation of RRP, the hybrid utilization of SF and RRP further mitigates the magnitude of compressive strength degradation in concrete specimens.

(4) The synergistic interaction between SF and RRP effectively reduces the porosity of concrete, amplifies the extent of mechanical property optimization induced by SF, and thereby contributes to the overall performance improvement of concrete. Specifically, SF alleviates the stress generated by pore water during F-T cycles through the fiber-matrix interfacial stress transfer mechanism; in contrast, RRP optimizes the concrete's pore structure, rendering the internal pore space more closed and isolated. The collaborative operation of these two distinct yet complementary mechanisms ultimately leads to a substantial improvement in the F-T resistance of concrete. This optimised combination is particularly suitable for load-bearing structures in cold regions—such as hydraulic engineering projects, road pavements, and bridge components—where it substantially extends the service life of concrete structures while reducing maintenance costs. Concurrently, it facilitates the resource recovery of waste tyres, effectively mitigating environmental pollution caused by tyre accumulation.

Acknowledgement: The Youth Innovation Team of Shaanxi Universities are acknowledged.

Funding Statement: This research is supported by Youth Innovation Team Research Project of Shaanxi Provincial Department of Education (Nos.: 22JP099, 24JP197), Xijing University School-Level Scientific Research Fund Project (No. 190203), and Open Research Fund Program of State Key Laboratory of Hydroscience and Engineering—Tsinghua University (No.: sklhse-2023-C-04).

Author Contributions: The authors confirm contribution to the paper as follows: Conceptualization, Xinzhan Li and Tao Luo; methodology, Wenwen Hu, Tao Luo and Li Li; funding acquisition, Wenwen Hu, Tao Luo and Li Li; data curation, Xinzhan Li; visualization, Xinzhan Li; writing—original draft preparation, Xinzhan Li; writing—review and editing, Wenwen Hu, Xinzhan Li, Tao Luo and Li Li; formal analysis, Xinzhan Li; validation, Xinzhan Li; investigation, Xinzhan Li; resources, Xinzhan Li; supervision, Tao Luo; project administration, Tao Luo. All authors reviewed and approved the final version of the manuscript.

Availability of Data and Materials: The datasets generated and/or analyzed during the current study are not publicly available but can be accessed upon reasonable request. Interested researchers should contact the corresponding author (Tao Luo) via [luotao19870426@126.com] to request data access, with a detailed description of the intended research use. Data sharing will be granted following the approval of the corresponding author and compliance with relevant ethical and institutional guidelines.

Ethics Approval: Not applicable.

Conflicts of Interest: The authors declare no conflicts of interest.

References

1. Li Z, Li S, Jiang C. A study on the mechanical properties and performance of fibrous rubberized concrete. Buildings. 2025;15(8):1245. doi:10.3390/buildings15081245.
2. Han X, Zhou S, Chen A, Feng L, Ji Y, Wang Z, et al. Analytical evaluation of stress-strain behavior of rubberized concrete incorporating waste tire crumb rubber. J Clean Prod. 2024;450:141963. doi:10.1016/j.jclepro.2024.141963.
3. Gu Z, Jiang Y, Ma Z, Shen P, Poon CS. A review on the utilization of recycled concrete powders: preparation, activity excitation and application. Mater Rep Solidwaste Ecomater. 2025;1:9520002. doi:10.26599/mrse.2025.9520002.
4. Mohammad MUI, Li J, Wu Y-F. Design and strength optimization method for the production of structural lightweight concrete: an experimental investigation for the complete replacement of conventional coarse aggregates by waste rubber particles. Resour Conserv Recycl. 2022;184(1):106390. doi:10.1016/j.resconrec.2022.106390.

5. Pal A, Ahmed KS, Hossain FZ, Alam MS. Machine learning models for predicting compressive strength of fiber-reinforced concrete containing waste rubber and recycled aggregate. J Clean Prod. 2023;423:138673. doi:10.1016/j.jclepro.2023.138673.
6. Nocera F, Wang J, Faleschini F, Demartino C, Gardoni P. Probabilistic models of concrete compressive strength and elastic modulus with rubber aggregates. Constr Build Mater. 2022;322(1):126145. doi:10.1016/j.conbuildmat.2021.126145.
7. Lv J, Han W, Zheng J, Lin S, Yuan S. Effects of basalt fibre and rubber particles on the mechanical properties and impact resistance of concrete. Structures. 2024;65(1):106677. doi:10.1016/j.istruc.2024.106677.
8. Yuan S, Zhang F, Du S, Li K, Luo J, Liu Y, et al. Research on the wear resistance and impact resistance of modified rubberized concrete. Phys Chem Earth Parts A/B/C. 2024;135:103680. doi:10.1016/j.pce.2024.103680.
9. Feng LY, Chen AJ, Liu HD. Effect of waste tire rubber particles on concrete abrasion resistance under high-speed water flow. Int J Concr Struct Mater. 2021;15(1):37. doi:10.1186/s40069-021-00475-8.
10. Azunna SU, Aziz FNAA, Rashid RSM, Bakar NBA. Review on the characteristic properties of crumb rubber concrete. Clean Mater. 2024;12:100237. doi:10.1016/j.clema.2024.100237.
11. Taheri BM, Ramezanianpour AM, Sabokpa S, Gapele M. Experimental evaluation of freeze-thaw durability of pervious concrete. J Build Eng. 2021;33:101617. doi:10.1016/j.jobe.2020.101617.
12. Liang W, Liu S, Liu H, Yang G, Gao Y. Effect of freeze-thaw cycles on bond properties at the FRP-concrete interface: experimental evaluation and machine learning prediction. Buildings. 2025;15(22):4038. doi:10.3390/buildings15224038.
13. Wan X, Luo L, Tian J, Lu J, Yan Z. Experimental investigation and strength prediction model for unsaturated concrete under the coupled action of freeze-thaw cycles and salt erosion. J Cold Reg Eng. 2026;40(1):04025057. doi:10.1061/jcrgei.creng-1073.
14. Li K, Du S, Zeng J, Luo H, Tao H, Liang W, et al. The influence of curing methods on the frost resistance and constitutive model of rubber-recycled concrete under seawater freeze-thaw cycles. Constr Build Mater. 2024;452(1):138918. doi:10.1016/j.conbuildmat.2024.138918.
15. Han X, Zhang Z, Wang D, Chen A, Ji Y, Wang Z, et al. Experimental study on freeze-thaw failure mechanism of rubberized concrete and analytical evaluation of the damage evolution. Constr Build Mater. 2025;480:141511. doi:10.1016/j.conbuildmat.2025.141511.
16. Richardson AE, Coventry KA, Ward G. Freeze/thaw protection of concrete with optimum rubber crumb content. J Clean Prod. 2012;23(1):96–103. doi:10.1016/j.jclepro.2011.10.013.
17. Li L, Li X, Wang B, Tao J, Shi K. A review on interfacial bonding behavior between fiber and concrete. J Build Eng. 2025;105:112455. doi:10.1016/j.jobe.2025.112455.
18. Jiang P, Chen Y, Wang W, Yang J, Wang H, Li N, et al. Flexural behavior evaluation and energy dissipation mechanisms of modified iron tailings powder incorporating cement and fibers subjected to freeze-thaw cycles. J Clean Prod. 2022;351:131527. doi:10.1016/j.jclepro.2022.131527.
19. Alekseev KN, Zakharov EV. Effect of cyclic freeze-thaw on dynamic impact resistance of fiber-reinforced concrete. J Min Sci. 2024;60(6):921–7. doi:10.1134/S1062739124060061.
20. Zhang L, Mo KH, Tan TH, Yong CL, Yap SP, Lee FW. Role of hydrogen peroxide and sodium lauryl sulfate in producing fiber-reinforced lightweight foamed phosphogypsum-based material. Mater Rep Solidwaste Ecomater. 2025;1:9520011. doi:10.26599/mrse.2025.9520011.
21. Zhao H, Liu H. Study on the bonding properties of hybrid fiber ordinary concrete and recycled concrete with BFRP bars under freeze-thaw cycles. J Adhes Sci Technol. 2025;39(16):2508–30. doi:10.1080/01694243.2025.2506709.
22. Li X, Xiong Z, Liu F, Tang Y, Chen H, Li L. Investigation and prediction of mechanical properties of hybrid fibers reinforced concrete incorporating eco-friendly aggregate of recycled rubber under freeze-thaw cycles. J Build Eng. 2026;118:114962. doi:10.1016/j.jobe.2025.114962.
23. Gasir H, Khalil MM, Elsalakawy TS, Mustafa TS. Torsional performance of rubberized concrete beams containing steel fibers and steel tiers. Structures. 2025;77:109118. doi:10.1016/j.istruc.2025.109118.
24. Banthia N, Majdzadeh F, Wu J, Bindiganavile V. Fiber synergy in Hybrid Fiber Reinforced Concrete (HyFRC) in flexure and direct shear. Cem Concr Compos. 2014;48:91–7. doi:10.1016/j.cemconcomp.2013.10.018.

25. Li L, Ma Z, Gao C, Sun A, Liu B, Pu B. Hybrid effect of nano-$CaCO_3$ and polypropylene fiber on fresh and hardened properties of alkali-activated material. J Mater Civ Eng. 2024;36(6):04024143. doi:10.1061/jmcee7.mteng-16701.
26. Pham NP, Toumi A, Turatsinze A. Effect of an enhanced rubber-cement matrix interface on freeze-thaw resistance of the cement-based composite. Constr Build Mater. 2019;207:528–34. doi:10.1016/j.conbuildmat.2019.02.147.
27. An N, Wang H, Wang P, Xu C, Liu M. Tension-compression anisotropic cohesion model for the interlayer interface of 3D-printed concrete compression specimens. J Build Eng. 2025;107:112800. doi:10.1016/j.jobe.2025.112800.
28. Han S, Xiao G, Tan W, Zhou A, Yu J, Ou J. Effect of axial compression ratio on seismic behavior of hybrid FRP-steel reinforced concrete columns. Eng Struct. 2025;335:120325. doi:10.1016/j.engstruct.2025.120325.